Neuroprotective efficacy of aminopropyl carbazoles in a mouse model of amyotrophic lateral sclerosis

Rachel Tesla[a], Hamilton Parker Wolf[a], Pin Xu[b], Jordan Drawbridge[b], Sandi Jo Estill[a], Paula Huntington[b], LaTisha McDaniel[a], Whitney Knobbe[b], Aaron Burket[b], Stephanie Tran[b], Ruth Starwalt[a], Lorraine Morlock[a], Jacinth Naidoo[a], Noelle S. Williams[a], Joseph M. Ready[a,1], Steven L. McKnight[a,1], and Andrew A. Pieper[a,b,1,2]

Departments of [b]Psychiatry and [a]Biochemistry, University of Texas Southwestern Medical Center, Dallas, TX 75390

Contributed by Steven L. McKnight, August 27, 2012 (sent for review July 25, 2012)

We previously reported the discovery of P7C3, an aminopropyl carbazole having proneurogenic and neuroprotective properties in newborn neural precursor cells of the hippocampal dentate gyrus. We have further found that chemicals having efficacy in this in vivo screening assay also protect dopaminergic neurons of the substantia nigra following exposure to the neurotoxin 1-methyl-4-phenyl-1,2,3,6-tetrahydropyridine, a mouse model of Parkinson disease. Here, we provide evidence that an active analog of P7C3, known as P7C3A20, protects ventral horn spinal cord motor neurons from cell death in the G93A-SOD1 mutant mouse model of amyotrophic lateral sclerosis (ALS). P7C3A20 is efficacious in this model when administered at disease onset, and protection from cell death correlates with preservation of motor function in assays of walking gait and in the accelerating rotarod test. The prototypical member of this series, P7C3, delays disease progression in G93A-SOD1 mice when administration is initiated substantially earlier than the expected time of symptom onset. Dimebon, an antihistaminergic drug with significantly weaker proneurogenic and neuroprotective efficacy than P7C3, confers no protection in this ALS model. We propose that the chemical scaffold represented by P7C3 and P7C3A20 may provide a basis for the discovery and optimization of pharmacologic agents for the treatment of ALS.

Amyotrophic lateral sclerosis (ALS), also known as Lou Gehrig's disease, is a relatively rare, adult-onset, rapidly progressive and fatal disease that involves degeneration of spinal cord motor neurons (1). This disorder causes muscle weakness and atrophy throughout the body, and patients with ALS ultimately lose all voluntary movement. The earliest parts of the body affected in ALS reflect those motor neurons that are damaged first. Regardless of the region of onset, however, muscle weakness and atrophy invariably spread to other parts of the body as the disease progresses. Although disease progression varies between individuals, most patients are eventually unable to stand or walk, get in or out of bed on their own, or use their hands and arms. Difficulty with chewing, swallowing, and breathing leads to progressive weight loss and increased risk of choking and aspiration pneumonia. Toward the end stages of disease, as the diaphragm and intercostal muscles weaken, most patients require ventilator support. Individuals with ALS most commonly die of respiratory failure or pneumonia within 2–5 y of diagnosis. There are no current treatments for ALS.

Approximately 20% of inherited cases of ALS, and 3% of sporadic cases, are associated with autosomal dominant mutations in the *SOD1* gene on chromosome 21 (2–4), and about 150 different mutations dispersed throughout the gene have been identified thus far (5). *SOD1* encodes cytosolic Cu/Zn superoxide dismutase, an antioxidant enzyme that protects cells by converting superoxide (a toxic free radical generated through normal metabolic activity of mitochondria) to hydrogen peroxide. Unchecked, free radicals damage both mitochondrial and nuclear DNA, as well as proteins within cells. In ALS linked to mutations in *SOD1*, cytotoxicity of motor neurons appears to result from a gain of toxic SOD1 function, rather than from loss of dismutase activity. Although the exact molecular mechanisms underlying toxicity are unclear, mutation-induced conformational changes in SOD1 lead to misfolding and subsequent aggregation of mutant SOD1 in cell bodies and axons (6–10). Aggregate accumulation of mutant SOD1 is thought to disrupt cellular functions and precipitate neuron death by damaging mitochondria, proteasomes, protein-folding chaperones, or other proteins (10).

Transgenic animal models of mutant SOD1, such as G93A-SOD1 mutant mice, are currently used for research into the pathogenic mechanisms thought to broadly underlie ALS. Mice hemizygous for the G93A-SOD1 transgene express 18 ± 2.6 copies of a form of *SOD1* found in some patients with inherited ALS (a substitution of glycine to alanine at codon 93). This was the first mutant form of *SOD1* to be expressed in mice and is the most widely used and well-characterized mouse model of ALS. Superoxide dismutase activity in these mice is intact, and the pathogenic effect of the mutant transgene appears to be gain of function, as is thought to occur in human patients (11). Death of motor neurons in these mice occurs in the ventral horn of the spinal cord and is associated with paralysis and muscle atrophy (12). Around 100 d of age, G93A-SOD1 mice characteristically experience the onset of paralysis in one or more limbs, due to loss of spinal cord motor neurons. Paralysis spreads rapidly throughout the body, culminating in death of 50% of the mice within 7 wk of disease onset.

We have previously reported the identification of a proneurogenic, neuroprotective aminopropyl carbazole (P7C3) discovered through a target-agnostic in vivo screen of postnatal hippocampal neurogenesis (13). Prolonged administration of P7C3 to mice suffering from pathologically high levels of neuronal apoptosis in the dentate gyrus (14) safely restored hippocampal structure and function with no observable physiologic side effects (13). Furthermore, extended administration of P7C3 to aged rats impeded hippocampal cell death and preserved cognitive ability as a function of terminal aging (13).

We have synthesized and characterized a variant of P7C3, known as P7C3A20, which has greater potency and proneurogenic efficacy than the parent compound. P7C3A20 differs structurally by replacement of the hydroxyl group at the chiral center of the linker with a fluorine and the addition of a methoxy group to the aniline ring. P7C3A20 also displays a more favorable toxicity profile than P7C3, with no hERG channel binding, histamine

Author contributions: R.T., H.P.W., P.X., N.S.W., J.M.R., S.L.M., and A.A.P. designed research; R.T., H.P.W., P.X., J.D., S.J.E., P.H., L. McDaniel, W.K., A.B., S.T., R.S., L. Morlock, J.N., N.S.W., and A.A.P. performed research; J.N. and N.S.W. contributed new reagents/analytic tools; R.T., H.P.W., P.X., J.D., L. Morlock, J.N., N.S.W., J.M.R., S.L.M., and A.A.P. analyzed data; and R.T., N.S.W., J.M.R., S.L.M., and A.A.P. wrote the paper.

The authors declare no conflict of interest.

Freely available online through the PNAS open access option.

[1]To whom correspondence may be addressed. E-mail: steven.mcknight@utsouthwestern.edu, joseph.ready@utsouthwestern.edu, or andrew-pieper@uiowa.edu.

[2]Present address: Department of Psychiatry, University of Iowa Carver College of Medicine, Iowa City, IA 52242.

This article contains supporting information online at www.pnas.org/lookup/suppl/doi:10.1073/pnas.1213960109/-/DCSupplemental.

receptor binding, or toxicity to HeLa cells (13, 15, 16). We have also found that Dimebon, an antihistaminergic drug that is reported to have anti-apoptotic and mitochondrial protective properties (17, 18), displays modest efficacy in the same biologic assays used to discover and characterize P7C3 and P7C3A20. However, it does so with substantially less potency and ceiling of efficacy (CoE) (13).

Armed with three related chemicals, one having very high proneurogenic activity (P7C3A20), one having intermediate activity (P7C3), and one having only modest activity (Dimebon), we initiated efficacy studies in two animal models of neurodegenerative disease. In our companion article (19), we report evidence of significant neuroprotective activity of P7C3A20 in a rodent model of Parkinson disease (PD). P7C3 exhibited intermediate activity in the PD animal model, and Dimebon showed no evidence of efficacy. The correlative activities of chemicals tested in the neurogenesis and PD assays were extended to eight additional analogs of P7C3. In every case, derivatives of P7C3 that were active in the neurogenesis assay were also active in the animal model of PD, and inactive variants were inactive in both assays (19).

Here, we have used the same approach to score the activities of P7C3A20, P7C3, and Dimebon in a model of neuron death outside of the brain. To address this question, we used G93A-SOD1 mutant mice, a model of ALS characterized by spinal motor neuron death associated with decreased motor functioning. As was observed for the rodent model of PD, we hereby report robust activity of P7C3A20 in the G93A-SOD1 mouse model of ALS, intermediate activity for P7C3, and no activity for Dimebon.

Results

Efficacy of Early Administration of P7C3 to G93A-SOD1 Mutant Mice Before Disease Onset. As an initial test of efficacy in this disease model, we intraperitoneally administered P7C3 to female G93A-SOD1 transgenic mice, using a treatment paradigm of 20 $mg{\cdot}kg^{-1}{\cdot}d^{-1}$ P7C3, with vehicle administered to siblings, starting at 40 d of age. This treatment scheme was selected on the basis of standard protocols for initial proof of concept screens in G93A-SOD1 mutant mice (20, 21). To control for transgene copy number, mice were sibling matched between treatment groups, per standard protocol (20), and quantitative PCR was performed to ensure that the copy number was maintained within the normal range. After initiation of P7C3 or vehicle treatment, date of onset of illness was determined by peak weight, and initial progression of disease was defined as the day at which mice fell to 10% below their maximum weight (20, 21). Mice were also assessed daily by a standard measure of neurological severity score ranging from 0 to 4, with a higher number reflecting greater neurologic impairment. In addition to weight loss, a score of 2 or greater for two consecutive days was also used as an indication of disease progression (20, 21). This score was determined blind to treatment group with the scoring system described in Fig. S1.

P7C3 treatment slowed disease progression in G93A-SOD1 mice, as indicated by delaying the time point at which mice dropped to 10% below their maximum weight (Fig. S1). Treatment with P7C3 also delayed the age at which G93A-SOD1 mice advanced to a neurological severity score of 2 (Fig. S1). Furthermore, P7C3 treatment improved performance in the accelerating rotarod task as a function of disease progression, indicating a slowing of progression of motor impairment (Fig. S1). This effect of slowing disease progression did not translate into increased survival of the animals, which is consistent with other interventions that have ameliorated disease symptoms in rodent models of ALS without improving survival (22–24).

Comparison of the Efficacy of Administration of P7C3A20, P7C3, and Dimebon at Disease Onset for Blocking Spinal Motor Neuron Cell Death in G93A-SOD1 Mutant Mice. On the basis of the promising results of early (day 40) administration of P7C3 to G93A-SOD1 mutant mice, we next sought to determine whether P7C3A20, P7C3, or Dimebon could protect ventral horn spinal motor neurons when administered at the expected time of disease onset (day 80) (20). We initiated administration of P7C3, P7C3A20, or Dimebon, each at a dose of 20 $mg{\cdot}kg^{-1}{\cdot}d^{-1}$, and analyzed motor neuron cell survival by staining lumbar spinal sections for choline acetyltransferase (ChAT). ChAT, the enzyme that synthesizes the neurotransmitter acetylcholine, serves as a marker for spinal cord motor neurons. All sections were counted blind to treatment group to quantify motor neuron survival, and five mice for each treatment group were analyzed at 90, 100, 110, and 120 d. Each treatment group was compared with its own sibling-matched group that received the corresponding vehicle.

As shown in Fig. 1, the wild-type bar represents the average number of spinal motor neurons in 110-d-old, vehicle-treated, wild-type littermate mice. Because survival of motor neurons did not differ between the various vehicle treatment groups within

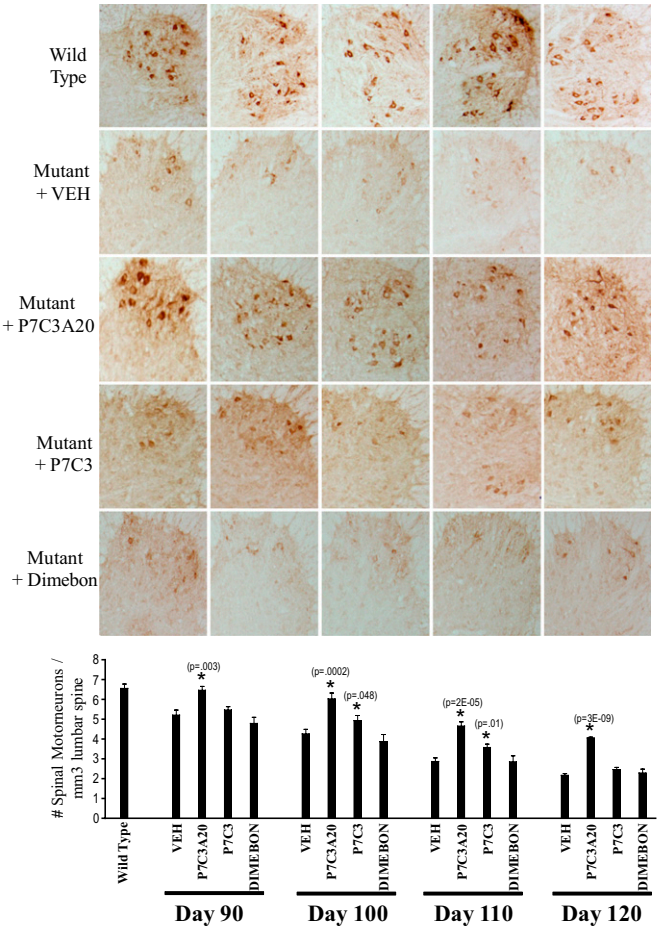

Fig. 1. P7C3A20 and P7C3 block motor neuron cell death in the spinal cord when administered at the time of disease onset to G93A-SOD1 mutant mice. Treatment of G93A-SOD1 mutant mice with 20 $mg{\cdot}kg^{-1}{\cdot}d^{-1}$ of P7C3A20, P7C3, or Dimebon, or the appropriate vehicle, was initiated on day 80. Five mice from each group were killed on days 90, 100, 110, and 120. The number of spinal cord motor neurons per cubic millimeter of lumbar spinal cord was determined through immunohistochemical staining for ChAT and quantification with National Institutes of Health Image J software. All images were analyzed blind to treatment group. Spinal cord motor neurons in G93A-SOD1 mutant mice died over time as expected. Spinal cord motor neuron cell death was blocked by administration of P7C3A20. P7C3 was intermediately protective, whereas Dimebon had no neuroprotective efficacy. (*Upper*) Representative staining of ChAT of one ventral horn from each of the five mice in each treatment group at 110 d is shown above the graph.

any given time point, the results were combined for ease of presentation. For animals expressing the G93A-SOD1 transgene, the number of spinal cord motor neurons steadily declined between days 90 and 120 (Fig. 1). At every time point, treatment with P7C3A20 provided significant protection from spinal motor neuron cell death (Fig. 1). Treatment with Dimebon revealed a rate of motor neuron loss indistinguishable from that of vehicle treatment groups. P7C3, by contrast, provided intermediate protection on days 100 ($P = 0.048$) and 110 ($P = 0.01$). By the time mice reached 120 d of age, however, the P7C3-treated group showed the same degree of motor neuron cell loss as vehicle and Dimebon-treated groups. Representative immunohistological staining of spinal cord sections is shown in Fig. 1 from each of the five mice examined on day 110. Taken together, these results demonstrate that daily administration of P7C3A20 starting at disease onset effectively blocks spinal motor neuron cell death in G93A-SOD1 mutant mice. P7C3 was active by these measures, but to a lesser extent than P7C3A20, whereas Dimebon was completely devoid of neuroprotective activity.

Comparison of the Efficacy of Administration of P7C3A20, P7C3, and Dimebon at Disease Onset for Preserving Rotarod Performance in G93A-SOD1 Mutant Mice. Having observed evidence of compound-mediated protection of spinal cord motor neurons, we next sought to determine whether motor performance might also be protected in these mice. Motor performance was monitored by the accelerating rotarod task standardly used for evaluation of rodent models of ALS (25, 26). We again initiated administration of P7C3, P7C3A20, or Dimebon on day 80, at 20 $mg{\cdot}kg^{-1}{\cdot}d^{-1}$, starting with no less than 20 mice per treatment group. Each animal in each group had its own sibling-matched vehicle control, and testing was conducted blind to treatment group. Rotarod training was initiated on day 50 for 2 d, and repeated weekly testing was conducted every 7 d thereafter. Each mouse was subjected to four trials of 600 s each, with a 20-min recovery break between each trial. The latency time to fall was averaged across all four trials.

As shown in Fig. 2, performance in all treatment groups was equal at weeks 10 and 11. Treatment with the test compounds was initiated midway between weeks 11 and 12, on day 80, and at

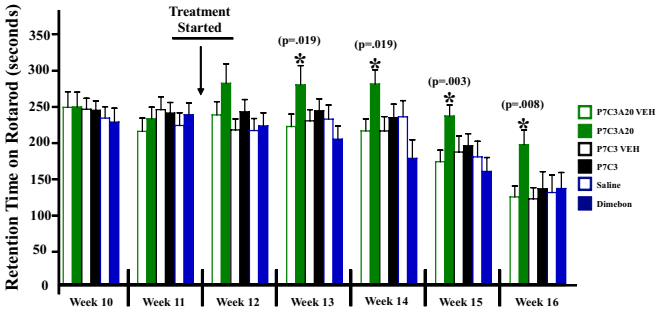

Fig. 2. P7C3A20 preserves performance in the accelerating rotarod test when administered at the time of disease onset to G93A-SOD1 mutant mice. Treatment of G93A-SOD1 mutant mice with 20 $mg{\cdot}kg^{-1}{\cdot}d^{-1}$ of P7C3A20, P7C3, or Dimebon, or the appropriate vehicle, was initiated on day 80, with 20 mice per group. All compounds were administered at 20 $mg{\cdot}kg^{-1}{\cdot}d^{-1}$ i.p. in divided doses. Each compound-treated mouse had a sex-matched sibling that received vehicle. Only sibling pairs were analyzed at each time point. By week 16, there were 13 compound–vehicle pairs remaining in each group. All vehicle-treated mice showed the expected decline in retention time on the accelerating rotarod over time, and P7C3 and Dimebon groups showed no difference in retention time compared with their vehicle groups. Mice treated with P7C3A20 showed significantly higher retention time on the rotarod at weeks 13, 14, 15, and 16. All testing and analysis were performed blind to treatment group.

week 12 there were no significant differences between groups. By week 13, however, P7C3A20-treated mice showed significantly better performance ($P = 0.019$) than the corresponding vehicle treatment group. In subsequent weeks, both P7C3 and Dimebon, as well as all vehicle groups, continued to decline at a steady pace in performance in this task, with P7C3A20-treated mice performing significantly better at each time point. Representative movies of P7C3A20- and vehicle-treated mice are shown in Movie S1. Rotarod data were not collected beyond week 16 because too few animals survived to this time point for valid comparison across groups.

As noted with early initiation of administration (day 40) of P7C3, this intervention improved rotarod performance but did not extend survival of the mice. Also, despite improvement in rotarod performance in P7C3A20-treated mice when daily treatment was initiated on day 80, we did not observe any delay in other measures of disease progression (neurological score or weight loss) (Fig. S2). This observation may reflect the increased challenge for efficacy associated with administering compounds at the time of disease onset. Taken together, our results show that administration at the time of disease onset of the most potent member of the P7C3 series of neuroprotective compounds, P7C3A20, significantly improves performance of G93A-SOD1 mice in the accelerating rotarod test. Both P7C3 and Dimebon were insufficiently active to preserve motor function in the accelerating rotarod task at 20 $mg{\cdot}kg^{-1}{\cdot}d^{-1}$ when administration was initiated at the time of disease onset.

Comparison of the Efficacy of Administration of P7C3A20, P7C3, and Dimebon at Disease Onset for Preserving Walking Gait in G93A-SOD1 Mutant Mice. Analysis of walking gait offers a second means of assessing motor limb strength and coordination in rodent models of ALS (25, 26). We conducted this analysis in the same mice used for the accelerating rotarod task, at three time points: 90, 118, and 132 d (Fig. S3). Briefly, the front paws of each test mouse were dipped in orange tempera paint and the back paws in blue tempera paint. Mice were then directed into a bisected PVC tube placed on top of artists' easel paper, such that the mouse was prompted to walk through the tunnel for a distance of 30 inches, leaving a trail of paw prints on the paper. Key parameters of the paw prints were then manually measured, as described in *Materials and Methods*. These parameters included front and back stride length, front and back width, and front-to-back paw distance (Fig. 3*A* and Fig. S4*A*).

Twenty total measurements (10 on each side) for each parameter were recorded per mouse, and 20 mice per group were evaluated at the 90- and 118-d time points. All measurements were conducted blind to treatment group. Front and back widths showed no difference as a function of treatment group or disease progression until day 132, at which point P7C3A20 treatment was observed to preserve back width (Fig. S4*B*). Three of the measured parameters (back stride, back-to-front distance, and front stride) showed significant improvement as a function of treatment with P7C3A20 earlier in the disease process, whereas none of these parameters in the walking gait analysis at 20 $mg{\cdot}kg^{-1}{\cdot}d^{-1}$ were significantly improved by treatment with P7C3 or Dimebon (Fig. 3*B*).

Back stride is defined as the distance between each successive back paw print on a single side, and one of the first features of disease in G93ASOD1 mutant mice is the onset of hind limb muscle weakness (20). As the disease progresses, mice are unable to move their hind limbs as much with each step, and back stride distance decreases. This was evident on day 118, in which P7C3, Dimebon, and all vehicle treatment groups showed reduced back stride length (Fig. 3*B*). Back stride measure was significantly ($P = 0.0016$) preserved to a near-normal level in P7C3A20-treated mice (Fig. 3*B*). Front stride is analogously defined as the distance between each successive front paw print

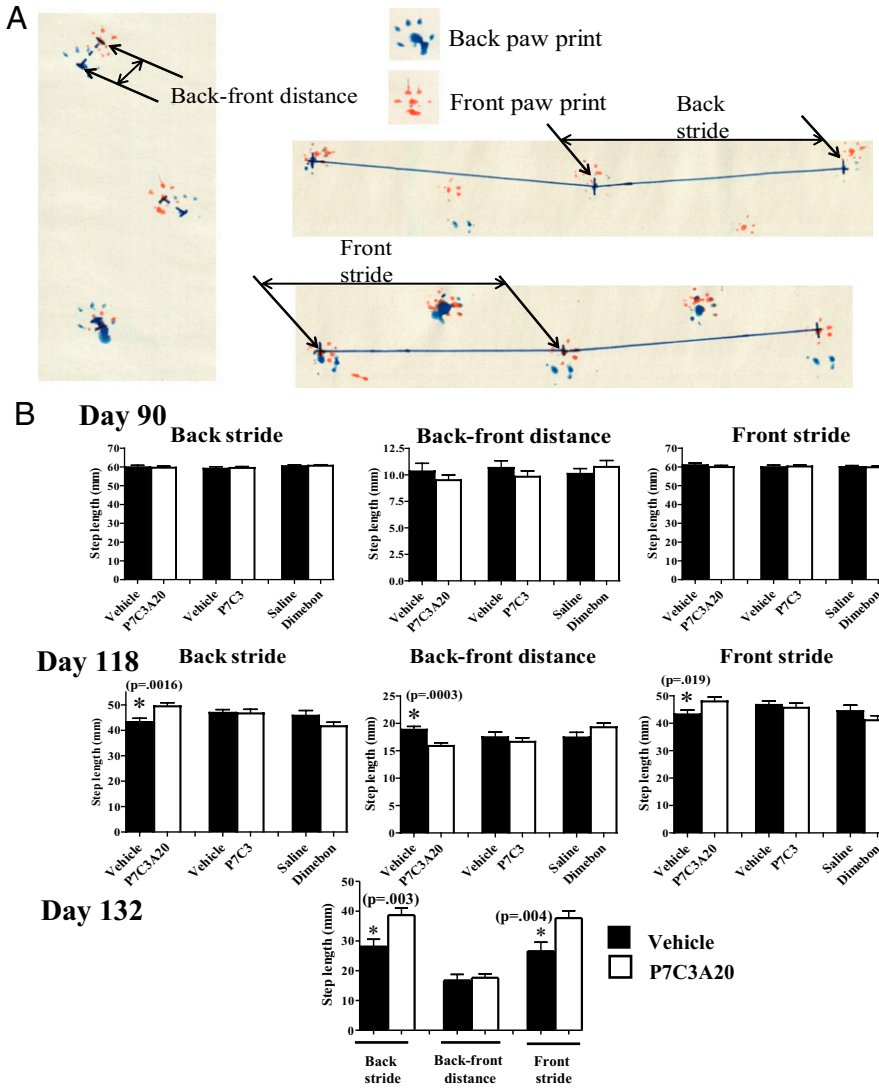

Fig. 3. P7C3A20 preserves walking gait when administered at the time of disease onset to G93A-SOD1 mutant mice. (*A*) The schematic diagram shows parameters used to measure gait. Front stride and back stride were collected as a straight line from back paw print to the following paw print. Back-to-front distance was collected as a straight line from back paw print to the corresponding front paw print. Twenty measurements (10 on each side) for each parameter were measured per mouse, and 20 mice per group were evaluated at 90- and 118-d time points. All measurements were conducted blind to treatment group, and Student's *t* test was used for statistical comparison of a treatment group to its matched vehicle group. (*B*) At 90 d, there were no differences between any groups in back stride, front stride, and back-to-front distance. By day 118, all vehicle groups, and P7C3- and Dimebon-treated mice, showed a significant difference in these measures, reflecting disease progression. Back stride and front stride were preserved to near-normal levels in P7C3A20-treated mice on day 118. By day 132, P7C3- and Dimebon-treated mice were too sick to participate in the task. At this time point, P7C3A20-treated mice continued to show normalized back stride and front stride levels.

on a single side, and as the disease progresses this measure also shortens as a consequence of the reduced hind limb stride that prevents the mouse from moving as great a distance with each step. Compromised front stride length thus confirms the deficit associated with back stride length, and we observed that on day 118 this measure was indeed reduced in P7C3, Dimebon, and all vehicle treatment groups, yet preserved to almost normal levels in P7C3A20-treated mice (Fig. 3*B*).

On day 132, there were insufficient numbers of mice in the P7C3-vehicle (P7C3-VEH) and Dimebon-VEH groups that could participate in the task, due to complete paralysis of one or more limbs in the majority of the original test group. In the A20-VEH group, however, there were still 10 P7C3A20 mice that were able to walk across the paper. Here, we observed that improvements in back stride and front stride were preserved, but there was no longer a difference in back-to-front distance. Back-to-front distance is defined as the distance between a back paw print and the front paw print on the same side. Early on, as the disease progresses in this animal model of ALS, the back-to-front distance steadily increases because the front limbs are able to extend normally, but the hindlimbs are not strong enough to formulate proper steps that should result in the back paw landing on top of the front paw print. It is evident in Fig. 3*B* that as assayed on day 118, treatment with P7C3A20 attenuated this increase in back-to-front distance. On day 132, however, the differences between VEH- and P7CA20-treated mice in back-to-front distance were lost. At this stage, the disease was sufficiently advanced that this measure reflects the additional complication of front limb weakness, such that the mice were unable to extend their front limbs normally. As a result, the back-to-front distance declined, and there were no differences between P7C3A20 and its sibling-matched vehicle group. Taken together, our results of gait analysis

demonstrate that treatment with P7C3A20 at the time of disease onset helps preserve walking gait in the G93A-SOD1 mouse model of ALS.

Analysis of Plasma, Brain, and Spinal Cord Levels of P7C3, P7C3A20, and Dimebon. Liquid chromatography-tandem mass spectrometry (LC/MS/MS) quantification of brain and blood levels of P7C3, P7C3A20, and Dimebon confirmed that all three compounds were able to enter both the brain and the spinal cord (Fig. 4). Notably, P7C3A20 displayed significantly greater protective efficacy compared with the other two compounds, despite the fact that P7C3A20 accumulated in spinal cord tissue at less than 1/20th the concentration of P7C3. Dimebon, which displayed no protective efficacy in G93A-SOD1 mice, showed comparable levels of spinal cord accumulation to those of P7C3A20. These results parallel findings observed in evaluation of the neuroprotective efficacy of these same three compounds in 1-methyl-4-phenyl-1,2,3,6-tetrahydropyridine (MPTP)-treated mice (19).

Discussion

The results of an unbiased screen of 1,000 chemically diverse, drug-like compounds led to the identification of an aminopropyl carbazole endowed with the capacity to enhance adult neurogenesis (2). This compound, designated P7C3, was found to act by blocking the death of newborn neurons in the dentate gyrus of adult mice. We have also found that P7C3, P73A20, and other active analogs protect dopamingergic neurons of the substantia nigra from MPTP-induced neurotoxicity (19). Here we have sought to determine whether this class of proneurogenic compounds might also block nerve cell death outside of the brain.

We selected P7C3, P7C3A20, and Dimebon for testing because they display distinct levels of proneurogenic, neuroprotective activity when assayed for protection from apoptotic cell death either of newborn hippocampal neurons (13) or following MPTP toxicity to mature dopaminergic neurons (19). P7C3A20 displays the highest potency and ceiling of efficacy among these three molecules. We evaluated Dimebon because of extensive studies in human clinical trials and its relative similarity in chemical structure to P7C3. When tested for its ability to protect mitochondrial membrane integrity following exposure of cultured cells to a calcium ionophore, Dimebon exhibited a protective potency between 100- and 1,000-fold lower than that of P7C3 (2). Similarly modest activity was observed when Dimebon was assayed in our standard model of hippocampal neurogenesis (2). The reduced potency and efficacy of Dimebon has been further revealed in its inability to protect dopaminergic neurons in the substantia nigra from MPTP toxicity (19). Finally, Dimebon has been extensively studied in human clinical trials of both Alzheimer's disease and Huntington disease. Although early indications in a phase 2 trial suggested that Dimebon might be efficacious for Alzheimer's disease (27), the drug failed in two independent phase 3 trials. By testing the properties of these three related compounds in the present study of protective efficacy in an animal model of ALS, we sought to determine whether the hierarchy of activities among these three molecules might be preserved.

Encouragingly, we observe that P7C3A20 significantly blocks death of spinal motor neurons in the G93A-SOD1 mouse model of ALS. Importantly this protective effect is observed when administration of the compound is initiated at the time of disease onset, and it correlates with preservation of muscle strength and coordination as assessed through the accelerating rotarod test and analysis of walking gait. P7C3 offered intermediate protection from cell death when administered at the time of disease onset. Administration of P7C3 for a prolonged period by initiating treatment much earlier (day 40) did preserve motor function as assayed by the accelerating rotarod task. Dimebon offered no protection in any of these measures. Although efficacy of Dimebon in an animal model of Alzheimer's disease (TGCRND8 mice) has recently been reported (28), this drug appears too weakly active to afford any protection in the G93A-SOD1 mutant mouse model of ALS.

We conclude that P7C3A20 and P7C3 display a hierarchy of activities analogous to their abilities to protect newborn hippocampal neurons from cell death (13), to block MPTP-mediated killing of mature dopaminergic neurons in the substantia nigra (19), and to protect spinal motor neurons from dying in G93A-SOD1 mutant mice. These collective observations give evidence that the relatively straightforward assay of monitoring adult hippocampal neurogenesis over a 7-d period following direct administration of unique analogs of P7C3 into the adult mouse brain may represent a trusted surrogate for the refinement of drug-like chemicals having neuroprotective activity. Over the past 2 y we have conducted a comprehensive structure–activity relationship (SAR) study to improve the chemical scaffold of the P7C3 series of molecules. To date, we have synthesized over 250 analogs of P7C3, all of which have been evaluated in the in vivo hippocampal neurogenesis assay. Our goal in these efforts to foster the discovery of a neuroprotective drug is to maximize neuroprotective efficacy and alleviate real or perceived vulnerabilities in the chemical structures. These efforts include, but are not limited to, eliminating the carbazole bromines, eliminating the aniline ring, increasing biologic activity, decreasing lipophilicity, eliminating any toxicities including hERG channel binding, increasing solubility, and reducing molecular weight. By use of the in vivo hippocampal neurogenesis assay, these ongoing SAR efforts with P7C3 analogs may offer an effective way to guide optimization of this series of molecules toward a neuroprotective drug candidate.

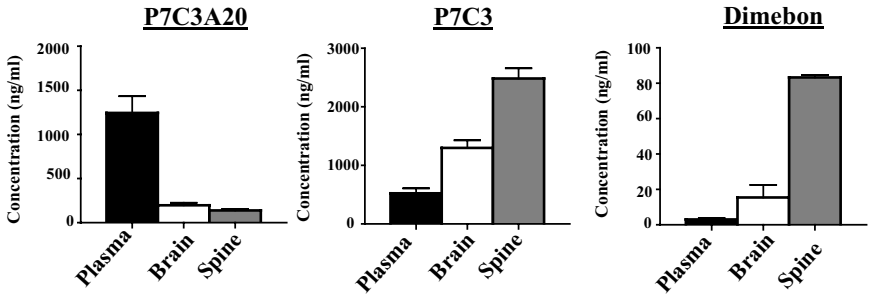

Fig. 4. Plasma, brain, and spinal cord levels of P7C3A20, P7C3, and Dimebon. Five mice for each compound group were treated for 21 d with 20 mg·kg^{-1}·d^{-1} of the compound, starting on day 85. Blood, brain, and spinal cord were harvested 6 h after the last injection and compound levels were measured by LC/MS/MS. Concentrations are presented as mean ± SEM.

No safely tolerated, neuroprotective chemical is available for the treatment of any form of neurodegenerative disease, including Parkinson disease, Alzheimer's disease, and amyotrophic lateral sclerosis. On the basis of the observations reported herein, we propose that a properly optimized variant of the P7C3 class of proneurogenic, neuroprotective chemicals may represent a viable candidate for the treatment of neurodegenerative disease.

Materials and Methods

Approval for the animal experiments described herein was obtained from the University of Texas Southwestern Medical Center Institutional Animal Care and Use Committee.

Statistics. All *P* values were obtained with Student's *t* test, by comparing treatment groups to their individual sibling-matched vehicle treatment groups.

Analysis of Motor Neuron Survival in the Spinal Cord. After transcardial perfusion with 4% (wt/vol) paraformaldehyde (PFA), the lumbar spinal cord was dissected and postfixed overnight in 4% PFA, cryoprotected in 30% sucrose at 4 °C, and then embedded in OCT and sectioned on a Thermo-Fisher cryostat (HM550) at 30-μm thickness. Every seventh section was immunohistochemically stained with goat anticholine acetyltransferase (anti-ChAT) (Millipore). Briefly, sections were incubated in 1% H_2O_2 for 45 min at room temperature, rinsed in Tris-buffered saline (TBS), and treated with 0.1% Triton-TBS and then blocked for 60 min in 3% BSA, 5% donkey serum, 0.3% Triton-100 in TBS. Sections were then incubated in goat anti-ChAT (1:100) in the same blocking solution overnight at 4 °C. The next day, sections were rinsed in TBS and incubated with donkey anti-goat biotin (1:200; Jackson ImmunoResearch). Signal was amplified with an ABC kit from Vector Labs, and diaminobenzidine was used as a chromagen. Immunostained tissue was then photographed at 4× using a Nikon Eclipse 90i motorized microscope, and the number of ChAT-positive neurons was counted in a blinded manner by two investigators, followed by normalization for ventral horn volume.

Rotarod. Rotarod testing was conducted as suggested in *Current Protocols in Neuroscience* (25, 26). An in-depth explanation of procedure can be found in *SI Materials and Methods*.

Paw Print Analysis. Paw prints were recorded at 90, 118, and 132 d of age. A 6 × 42-inch PVC pipe cut in half lengthwise was placed on top of a piece of easel paper (27 × 30 × 1/4 inches). Each mouse had paws covered in nontoxic tempera paint (orange in front, blue in back) and was placed at one end of the pipe. The mouse ran quickly to the other end of the pipe when released, and the procedure was repeated until 10 clear back and front prints were made for each side while the subject was running. Paw prints were scanned using a hand scanner and then visualized for measurement in Nikon Metamorph software. Measurements were based on established guidelines (25, 26). An in-depth explanation of procedure can be found in *SI Materials and Methods*.

Neurological Scoring. Neurological scoring was based on established guidelines (20, 21). An in-depth explanation of procedure can be found in *SI Materials and Methods*.

Weight Data. Mice were weighed daily starting on the day of initiation of compound administration to assess disease progression and readjust compound dosage. A digital balance with a step of 0.01 g was used, and mice were placed in a small plastic container on the scale when weighed. Weight was taken between 11:00 AM and 1:00 PM every day.

Quantitative PCR. Quantitative PCR was done in accordance with guidelines established by the Jackson Laboratory protocol for SOD1-G93A mice.

Synthesis and Preparation of P7C3A20. Preparation of compound was as described by Pieper et al. (13).

Pharmacokinetic Analysis of P7C3, P7C3A20, and Dimebon. Analysis of compound was as described by Pieper et al. (13). An in-depth explanation of procedure can be found in *SI Materials and Methods*.

ACKNOWLEDGMENTS. We thank Jeannie Zhong and Vy Thuy Ho for technical assistance and Drs. Jay Baraban, Martin Raff, and Dale Boger for critical review of the manuscript. This work was supported by grants from The Edward N. and Della C. Thome Memorial Foundation and the Welch Foundation (I-1612) (to J.M.R.); the Ted Nash Long Life Foundation, The Hartwell Foundation, the Staglin Family Fund, and the Morton H. Meyerson Family Tzedakah Fund (A.A.P.); a National Institutes of Health transformative R01 grant (National Institute of Mental Health Grant R01MH087986) (to A.A.P. and S.L.M.); National Cancer Institute Program Project Grant P01CA095471 (to S.L.M.); and funds provided by an anonymous donor (to S.L.M.).

1. Tandan R, Bradley WG (1985) Amyotrophic lateral sclerosis: Part 1. Clinical features, pathology, and ethical issues in management. *Ann Neurol* 18:271–280.
2. Valdmanis PN, Daoud H, Dion PA, Rouleau GA (2009) Recent advances in the genetics of amyotrophic lateral sclerosis. *Curr Neurol Neurosci Rep* 9:198–205.
3. Rosen DR, et al. (1993) Mutations in Cu/ZN superoxide dismutase gene are associated with familial amyotrophic lateral sclerosis. *Nature* 364:59–62.
4. Shaw CE, et al. (1997) Familial amyotrophic lateral sclerosis. Molecular pathology of a patient with a SOD1 mutation. *Neurology* 49:1612–1616.
5. Valentine JS, Doucette PA, Zittin Potter S (2005) Copper-zinc superoxide dismutase and amyotrophic lateral sclerosis. *Annu Rev Biochem* 74:563–593.
6. Bruijn LI, et al. (1998) Aggregation and motor neuron toxicity of an ALS-linked SOD1 mutant independent from wild-type SOD1. *Science* 281:1851–1854.
7. Furukawa Y, Fu R, Deng HX, Siddique T, O'Halloran TV (2006) Disulfide cross-linked protein represents a significant fraction of ALS-associated Cu, Zn-superoxide dismutase aggregates in spinal cords of model mice. *Proc Natl Acad Sci USA* 103: 7148–7153.
8. Prudencio M, Hart PJ, Borchelt DR, Andersen PM (2009) Variation in aggregation propensities among ALS-associated variants of SOD1: Correlation to human disease. *Hum Mol Genet* 18:3217–3226.
9. Wang Q, Johnson JL, Agar NY, Agar JN (2008) Protein aggregation and protein instability govern familial amyotrophic lateral sclerosis patient survival. *PLoS Biol* 6: e170.
10. Boillée S, Vande Velde C, Cleveland DW (2006) ALS: A disease of motor neurons and their nonneuronal neighbors. *Neuron* 52:39–59.
11. Valentine JS, Hart PJ (2003) Misfolded CuZnSOD and amyotrophic lateral sclerosis. *Proc Natl Acad Sci USA* 100:3617–3622.
12. Gurney ME, et al. (1994) Motor neuron degeneration in mice that express a human Cu,Zn superoxide dismutase mutation. *Science* 264:1772–1775.
13. Pieper AA, et al. (2010) Discovery of a proneurogenic, neuroprotective chemical. *Cell* 142:39–51.
14. Pieper AA, et al. (2005) The neuronal PAS domain protein 3 transcription factor controls FGF-mediated adult hippocampal neurogenesis in mice. *Proc Natl Acad Sci USA* 102:14052–14057.
15. MacMillan KS, et al. (2011) Development of proneurogenic, neuroprotective small molecules. *J Am Chem Soc* 133:1428–1437.
16. McKnight SL, Pieper AA, Ready JM, De Brabander J (2010) Proneurogenic Compounds. US Patent 2010/020681.
17. Bachurin S, et al. (2001) Antihistamine agent Dimebon as a novel neuroprotector and a cognition enhancer. *Ann N Y Acad Sci* 939:425–435.
18. Bachurin SO, Shevtsova EP, Kireeva EG, Oxenkrug GF, Sablin SO (2003) Mitochondria as a target for neurotoxins and neuroprotective agents. *Ann N Y Acad Sci* 993: 334–344, discussion 345–349.
19. De Jesús-Cortés H, et al. (2012) Neuroprotective efficacy of aminopropyl carbazoles in a mouse model of Parkinson disease. *Proc Natl Acad Sci USA* 109:17010–17015.
20. Letiner M, Menzies S, Lutz C (2010) *Working with ALS mice. Guidelines for Preclinical Testing & Colony Management* (The Jackson Laboratory, Bar Harbor, ME).
21. Ludolph AC, et al.; ENMC Group for the Establishment of Guidelines for the Conduct of Preclinical and Proof of Concept Studies in ALS/MND Models (2007) Guidelines for the preclinical in vivo evaluation of pharmacological active drugs for ALS/MND: Report on the 142nd ENMC international workshop. *Amyotroph Lateral Scler* 8:217–223.
22. Da Cruz S, et al. (2012) Elevated PGC-1α activity sustains mitochondrial biogenesis and muscle function without extending survival in a mouse model of inherited ALS. *Cell Metab* 15:567–569.
23. Kariya S, et al. (2012) Mutant superoxide dismutase 1 (SOD1), a cause of amyotrophic lateral sclerosis, disrupts the recruitment of SMN, the spinal muscular atrophy protein to nuclear Cajal bodies. *Hum Mol Genet* 21:3421–3434.
24. Rouaux C, et al. (2007) Sodium valproate exerts neuroprotective effects in vivo through CREB-binding protein-dependent mechanisms but does not improve survival in an amyotrophic lateral sclerosis mouse model. *J Neurosci* 27:5535–5545.
25. Carter RJ, Morton J, Dunnet SB (2001) Motor coordination and balance in rodents. *Curr Protoc Neurosci* 8.12. Available at www.currentprotocols.com.
26. Jackson M, Ganel R, Rothstein JD (2002) Models of amyotrophic lateral sclerosis. *Curr Protoc Neurosci* 9.13. Available at www.currentprotocols.com.
27. Doody RS, et al.; dimebon investigators (2008) Effect of dimebon on cognition, activities of daily living, behaviour, and global function in patients with mild-to-moderate Alzheimer's disease: A randomised, double-blind, placebo-controlled study. *Lancet* 372:207–215.
28. Steele JW, et al. (2012) Latrepirdine improves cognition and arrests progression of neuropathology in an Alzheimer's mouse model. *Mol Psych*, 10.1038/mp.2012.106.